ACS OMEGA

Open Access

http://pubs.acs.org/journal/acsodf

Article

Recycling Motorcycle Exhaust Soot into Fluorescent Graphene Oxide Quantum Dots for Sensing Ferrocyanide Ions and Bioimaging Cells: A Method for Waste Utilization

Chanchal Das, Nasim Sepay, Tae Wan Kim, Shinwon Chae, Nandan Ghosh, Mohan Dumpala, Dongsic Choi, Seob Jeon, Jungkyun Im,* and Goutam Biswas*

Cite This: *ACS Omega* 2025, 10, 14229−14240

Read Online

ACCESS | Metrics & More | Article Recommendations | Supporting Information

ABSTRACT: Graphene oxide quantum dots (GOQDs) with a high quantum yield (50%) were synthesized using soot collected from a motorcycle (petroleum vehicle) exhaust pipe and applied as sensors for ferrocyanide ($[Fe(CN)_6]^{4-}$) ions and as bioimaging agents in a cancer cell line. X-ray photoelectron spectroscopy (XPS) data for the GOQDs revealed a C/O ratio of 2.49, which was close to that of graphene oxide (GO). The synthesized GOQDs exhibited strong blue fluorescence. High sensitivity to detect $[Fe(CN)_6]^{4-}$ was reported in GOQDs with a detection limit of 0.46 nmol mL^{-1}, and a strong linear relationship was achieved in the concentration range of 100−1100 $\mu g\ L^{-1}$. The results demonstrate the utility of GOQDs for detecting $[Fe(CN)_6]^{4-}$ in a real scenario. The GOQDs exhibited almost negligible cytotoxicity in cells and were internalized within 4 h of incubation, emitting blue fluorescence in the cytoplasm. This suggests that the GOQDs are promising bioimaging agents for biomedical applications. In general, these waste-derived GOQDs appear to be good chemo- and biosensing probes for real-life applications.

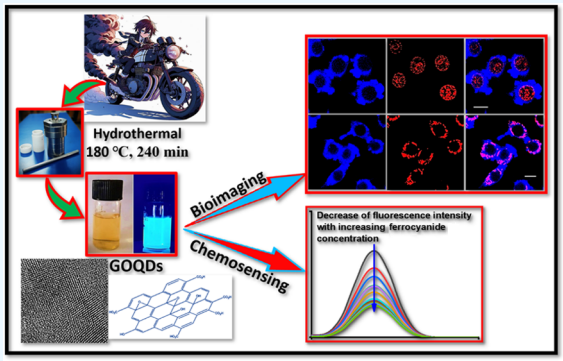

1. INTRODUCTION

Urbanization and population growth have contributed to an increase in waste diversity, necessitating enhanced strategies for waste disposal and management to maintain cleaner environments. These wastes include paper, agriculture, food, yard trimming, animal, glass, plastic, metal, leather, rubber, textiles, and wood.[1] Developing countries face challenges in disposing large amounts of waste, leading to the need for sustainable, cost-effective, ecological, social, and legally permissible management. Waste rich in proteins, minerals, carbohydrates, and carbon can be used as raw materials in material science.[2] For example, eggshell membranes, which are rich in proteins, are converted into carbon nanodots by microwave-assisted carbonization.[3] In another example, carbon quantum dots (CQDs) were made from sugar cane bagasse pulp (rich in carbohydrates) using a hydrothermal technique.[4] Carbohydrate-rich watermelon peel was used to synthesize the fluorescent carbon dots .[5] Here, we recycled fuel (petroleum) waste to make graphene oxide quantum dots using an easy and greener method.

Nanotechnology has provided a new approach in the field of applied science. which includes areas like environmental energy,[6] catalysis,[7] food safety,[8] medicines, biotechnology, sensors, electronics, and optics.[9−17] In recent years, nanomaterials have held the potential to create ground-breaking technologies in the health sciences.[18] Various carbon-based nanomaterials are one of them and important for sensor applications.[19] Carbon-based materials, including carbon nanotubes, fullerenes, graphenes,[20−22] graphene oxide, carbon onions, carbon nanoribbons, graphene quantum dots, carbon quantum dots, and graphene oxide quantum dots, have been employed in the field of bio/chemosensors,[23−25] cancer treatment,[26,27] and several other uses.[28−32] Graphene oxide quantum dots (GOQDs) are a type of carbon-based quantum dots with exceptional photoluminescence characteristics that make them attractive for applications such as nanoprobes and bioimaging. Research has been conducted to enhance the properties of GOQDs and broaden their range of applications. GOQDs have shown outstanding quality and have diverse applications in sensing and cytotoxicity research. The current study explored the biosensing, cytotoxicity, and chemo-sensitivity of GOQDs. HeLa is a cervical cancer cell line, whereas HepG2 is a liver cell line isolated from a hepatocellular carcinoma. The International Cell Line

Received: January 9, 2025
Revised: March 12, 2025
Accepted: March 17, 2025
Published: March 31, 2025

Authentication Committee (ICLAC) identified 488 contaminated cell lines, with 116 cases caused by HeLa cells, accounting for 24% of all known contaminated cell lines.[33] Bioimaging techniques such as photoacoustic, X-ray, MRI, and PET are used; however, they have drawbacks such as dangerous radioactive materials, slow operation, and skilled operators.[34] Nanomaterials, such as gold nanoparticles, have good sensing abilities but are expensive. In addition, most current methods, such as MRI, are expensive and time-consuming. Current sensing processes involve complicated instrumentation setups, high temperatures, highly skilled operators, and a small detection range of the solution pH.[35,36] Therefore, a more sophisticated and cheaper method is required for accurate detection of harmful cancer cells. In this regard, quantum dots can be efficient candidates, especially GOQDs, because they have very good solubility in water, excellent chemical stability, low toxicity, and good photostability. GOQDs have a large number of oxygen-containing functional groups, which can be easily functionalized by various fluorophores.[37] Hence, biosensing was applied to HeLa cells and cytotoxicity was assessed in HeLa and HepG2 cell lines.

Ferrocyanide ions ($[Fe(CN)_6]^{4-}$) are used in caking processes, while sodium, potassium, and calcium ferrocyanides are used as anticaking agents. Ferrocyanide ions are less toxic but can break down at high temperatures, forming highly toxic cyanides and converting them to sodium cyanide or virulent hydrocyanic acid under alkaline and acidic conditions, causing health risks. Improper use can cause Parkinson's disease (PD), mental deterioration, and neurodegenerative diseases. Food-grade salts in the European Union (20 mg/kg),[38] United States (13 mg/kg),[38] China (10 mg/kg),[39] and Japan (<20 mg/kg)[38] have different safe dosages. Therefore, it is crucial to develop an accurate analytical approach for the detection of ferrocyanide in food. Various methods have been developed, but most of them have different drawbacks, as previously discussed. Therefore, a spectrofluorimetric approach based on quantum dots may be effective for detecting ferrocyanide; however, more research is needed to fully exploit its benefits.

Based on this knowledge, we hypothesized using novel recycled fuel waste-derived GOQDs as biosensors (toward HeLa cells) and, at the same time, as a sensitive fluorescent nanoprobe for the detection of $[Fe(CN)_6]^{4-}$ ions. The fluorescence intensity of the GOQDs exhibited considerable imaging of the respective cell lines along with a quenching effect from $[Fe(CN)_6]^{4-}$. The synthesized GOQDs were used in HeLa and HepG2 cell lines to test their cytotoxicity. Our proposed fluorescence approach is expected to open new avenues for applications in cancer diagnosis and food quality monitoring.

2. EXPERIMENTAL SECTION

2.1. Materials. All chemicals were of analytical grade and obtained from Sigma-Aldrich. Milli-Q water was used for the preparation of each solution and synthesis. MitoTracker Red CMXRos and DRAQ5 were purchased from Thermo Fisher Scientific (Invitrogen). The optical properties were characterized using an ultraviolet−visible (UV−vis) spectrometer (Thermo Scientific Evolution 201) and fluorescence spectrometer (Hitachi, F-2700). Structural analysis was performed using Fourier-transform infrared (FTIR) spectroscopy, and the morphology of the GOQDs was analyzed using high-resolution transmission electron microscopy (HRTEM) (JEM-F200, JEOL).

2.2. Synthesis of GOQDs. Briefly, soot was collected from a petrol-based motorcycle exhaust pipe. To synthesize GOQDs, petrol-based motorcycle exhaust soot was collected and thoroughly dried. Then, 12 mL of H_2O_2 solution [5% (w/w)] was added to 120 mg of dried soot and heated at 180 °C in a 25 mL Teflon-lined autoclave for 240 min. After cooling, filtration was performed using Whatman No. 1 filter paper (to remove the unreacted carbon source), followed by centrifugation at 15,000 rpm for 7 min to obtain a clear and light straw yellow-colored solution. Under 365 nm UV light, this solution produced strong blue fluorescence. The obtained straw-yellow-colored GOQD solution was treated under reduced pressure and heat to obtain solid GOQDs. The yield of the solid GOQDs was approximately 11% by weight. The solid GOQDs were wrapped in aluminum foil (to protect them from light) and stored at 0−4 °C.

2.3. Detection of $[Fe(CN)_6]^{4-}$ Ions. To demonstrate the chemosensing ability of the synthesized GOQDs, various concentrations of $[Fe(CN)_6]^{4-}$ were mixed and monitored by fluorometry. $K_4[Fe(CN)_6]$ solutions with various concentration (0−1100 μg L^{-1} or ng mL^{-1}) were prepared in Milli-Q water. A 150 mg L^{-1} or 150 ng mL^{-1} suspension of the nanoprobes was created by adding 20 mL of Milli-Q water to 3 mg of GOQDs. Each concentration of $[Fe(CN)_6]^{4-}$ was added to 1 mL of 150 mg L^{-1} GOQDs solution. LOD and LOQ were calculated using the equations given below (eqs 1−2)

$$\mathrm{LOD} = 3.3 \times \frac{\mathrm{SD}_i}{m} \tag{1}$$

$$\mathrm{LOQ} = 10 \times \frac{\mathrm{SD}_i}{m} \tag{2}$$

where SD_i = Standard deviation of the intercept in the calibration curve and m is the slope of the calibration curve.

After mixing the $[Fe(CN)_6]^{4-}$ solution with the GOQDs solution, photoluminescence (PL) intensity was recorded at 418.5 nm with λ_{ex} = 308.5 nm.

2.4. Cellular Uptake Study by Confocal Microscopy. For the cellular uptake study, HeLa cells were seeded on a 35 mm cover glass-bottomed dish (SPL Ltd., Pocheon, Korea) at a concentration of 2×10^4 cells/dish. After incubation for 24 h and removal of the cell culture media, GOQDs (0.1 mg mL^{-1}) in serum-free media were added, and the cells were incubated for 4 h at 37 °C. The cells were then washed three times with PBS to remove any noninternalized GOQDs, and either 2 mL of DRAQ5 (10 μM) or 2 mL of MitoTracker (100 nM) was added and incubated for 10 min to stain the nucleus or mitochondria. Confocal laser scanning microscopy (Carl Zeiss LSM 710) with an oil immersion lens (NA 1.30, 100X) was used to detect the fluorescence inside the cells. The GOQDs were excited at 405 nm using a HeNe laser and blue fluorescence was observed at 426−500 nm. DRAQ5 and Mito Tracker were excited at 543 nm and red fluorescence was observed at 649−808 nm.

2.5. Evaluation of Cytotoxicity of GOQD by 3-(4,5-Dimethylthiazol-2-yl)-2,5-diphenyltetrazolium Bromide (MTT) Assay. HeLa and HepG2 cells were seeded in 96-well plates at a density of 1×10^4 cells/well in DMEM containing 10% fetal bovine serum (FBS, Welgene) and 1% penicillin-streptomycin (Hyclone). After 24 h of culturing at 37 °C in a CO_2 incubator, the culture media were removed and the cells

https://doi.org/10.1021/acsomega.5c00229
ACS Omega 2025, 10, 14229−14240

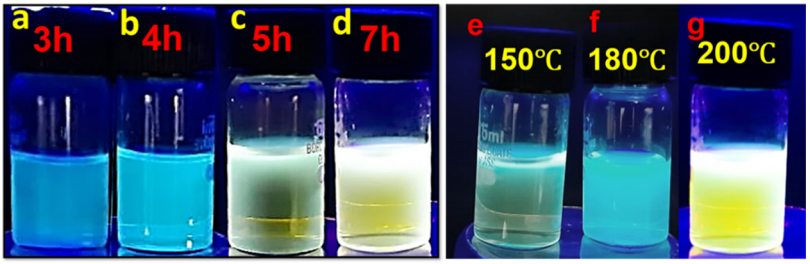

Figure 1. Emissive light under 365 nm for the synthesized GOQDs at various time length: (a) 3 h, (b) 4 h, (c) 5 h, (d) 7 h and temperatures: (e) 150 °C, (f) 180 °C, (g) 200 °C.

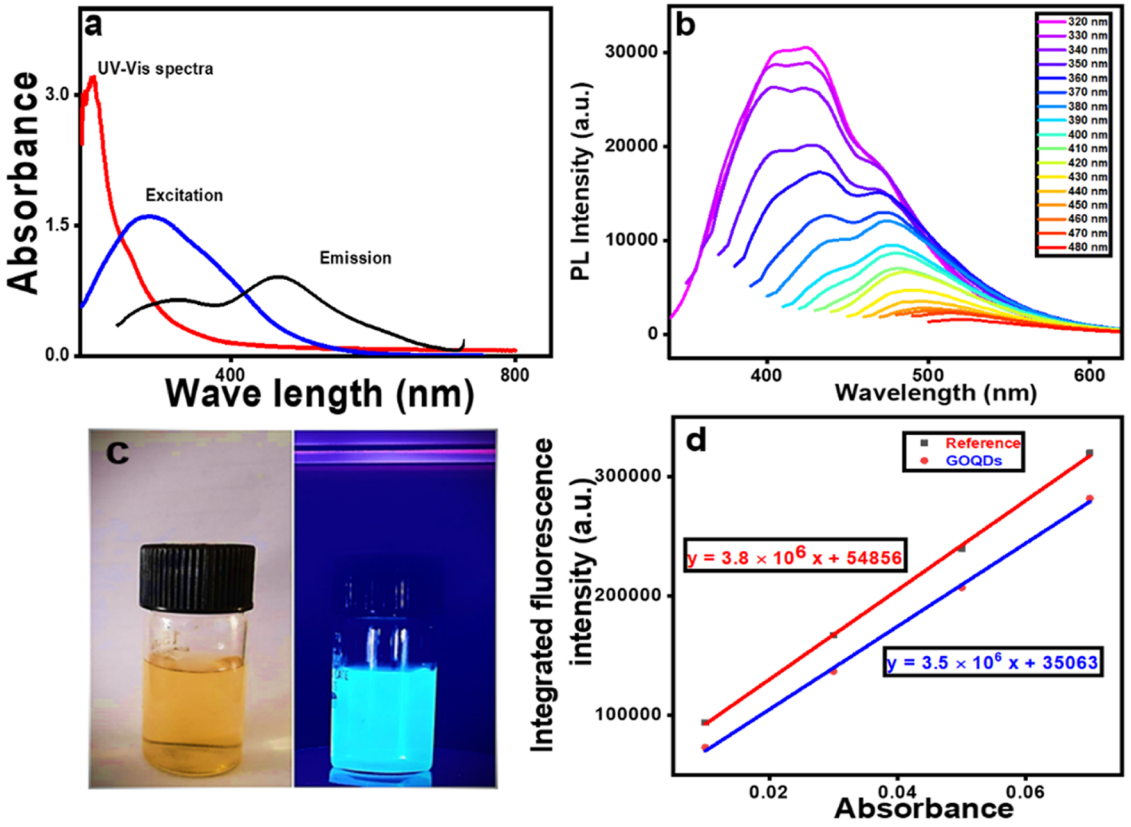

Figure 2. (a) UV−vis, excitation, and emission spectra; (b) PL spectra. (c) Aqueous suspension before (left vial) and after (right vial) irradiation with UV-365 nm light. (d) Integrated fluorescence intensity vs absorbance plots for GOQDs and quinine sulfate (reference).

were washed with 200 μL of PBS. The GOQDs solutions were treated with different concentrations ranging from 0 to 250 μg mL^{-1} in serum-free medium and incubated for 24 h at 37 °C. The treated cells were rinsed with cold PBS and exposed to MTT with media for 4 h. The media were removed, and DMSO (180 μL) was added to each well to dissolve the formazan crystals. The dissolved formazan was quantified using VICTOR Nivo, Multimode plate reader to measure its spectrophotometric absorbance at 540 nm. The percentage of cytotoxicity was calculated based on the control (0 μg mL^{-1} GOQD). All MTT assay experiments were conducted in triplicate.

3. RESULT AND DISCUSSION

3.1. Synthesis of GOQDs. Upon extending the reaction time from 4 to 7 h, the emission of the synthesized GOQDs under 365 nm irradiation transitioned from blue to lemon-yellow (Figure 1a−d). Optimal blue fluorescence was observed when the reaction time was increased from 3 to 4 h, transitioning to light lemon-yellow begins after 5 h, and reached maximum brightness after 7 h. Additionally, the synthesis temperature of the GOQDs was varied at 150, 180, and 200 °C for 4 h (Figure 1e−g). The results indicated that the synthesized GOQDs exhibited the most intense blue emission when the temperature was increased from 150 to 180 °C, with further heating resulting in GOQDs that emitted lemon-yellow light emission.

In general, as the reaction time increases, there is a greater probability of aggregate formation or surface oxidation, resulting in a shift from blue to bright lemon-yellow light. As the temperature increases, surface oxidation occurs, resulting in an increase in the number of oxygen-containing groups on the surface; thus, a redshift takes place.[40] As mentioned in a previous study, aggregation leads to a larger size, and with increasing size, red shifting occurs, which is also observed here.[41]

3.2. Characterization Techniques. Various characterization techniques can be applied to obtain concrete evidence

https://doi.org/10.1021/acsomega.5c00229
ACS Omega 2025, 10, 14229−14240

Table 1. Various Parameters for the QY Calculation of GOQDs

sl no.	concentrations (% v/v)	UV absorbance	area of PL spectra (GOQDs)	area of PL spectra (Reference)
1	25%	0.01	72,708	93,714.7
2	50%	0.03	136,699.7	166,833.3
3	75%	0.05	206,827.9	239,663
4	100%, 61 mg L^{-1}	0.07	281,701.4	319,600
QYs (%) Solvent = Water			slope = 3.5 × 10^6, intercept = 35,063	slope = 3.8 × 10^6, intercept = 54,856
			50.3%	54.6% (reported)

for the formation of GOQDs. These methods can be categorized into three groups: morphological, skeletal, and optical. For optical characterization, a dilute suspension of the materials was characterized using UV−vis and fluorescence spectroscopy. FTIR spectra and XPS analysis can be used for skeletal or structural characterization, and HRTEM analysis can be used to study morphological properties.

3.2.1. Study of Optical Properties. The optical characteristics of the GOQDs were identified by UV−vis and PL spectroscopy, and the results are shown in Figure 2a,b. The UV−vis absorption spectra of the GOQDs exhibited a wide absorption from 190 to 800 nm with one peak at 207.5 nm and two shoulders at 261 and 336 nm. According to the literature, the 207.5 nm transition is due to the π-π^* of aromatic C═C, while the transition for the n-π^* of the C═O bond occurs at 261 nm. A similar result was also found by Nugroho et al.[42] for GOQDs. The PL spectra show peak intensities at various excitation wavelengths, as illustrated in Figure 2b, which reveals that the fluorescence of the produced GOQDs is excitation dependent. From the results, it can be clearly observed that with increasing excitation wavelength, the emission intensity decreases and is maximized at 320 nm; hence, a 320 nm excitation wavelength was used in every case. Figure 2b also illustrates that when the excitation wavelength increased from 320 to 480 nm, the emission peak shifted toward longer wavelengths. This may be due to surface flaws, more oxygen-containing functional groups, different particle sizes, and emissive trap energy levels, which are also responsible for the carbon dot type.[43,44] The maximum emission intensity at 320 nm is in the range of 408−420 nm. Figure 2c shows the suspension of GOQDs under daylight and UV-365 nm light. Strong blue-emissive light was observed under 365 nm UV light.

The quantum yield (QY) for the GOQDs were calculated by comparing the respective PL spectra of all aqueous GOQDs with that of quinine sulfate using the following formula given as eq 3.[45,46] For the GOQDs and quinine sulfate, the QY (φ_{GOQDs}) was estimated by plotting the integrated fluorescence intensity against the absorbance (Figure 2d), and the resulting slope is used in eq 3

$$\varphi_{GOQDs} = \varphi_{ref} \times \frac{m_{GOQDs}}{m_{ref}} \times \frac{\eta_{GOQDs}}{\eta_{ref}} \quad (3)$$

where φ_{GOQDs}, φ_{ref} = QY, m_{GOQDs}, m_{GOQDs} = slopes of Figure 2d, η_{GOQDs}, η_{ref} = optical density of GOQDs, and quinine sulfate. The QY calculation results are presented in Table 1.

The QY of the synthesized GOQDs was calculated and found to be approximately 50% with respect to quinine sulfate as the reference fluorophore, which had a QY of 54.6%. A comparison of the QY of various biomass-derived carbon dots and our reported GOQDs is presented in Table 2. From the table, it can be said that our synthesized GOQDs had a much better QY than the other reported materials; hence, this was used to sense ferrocyanide ions and for bioimaging purposes.

Table 2. Comparison with Various Reported Carbon-Based QD Showing Blue Fluorescence

biomass source	type of QDs	QY (%)	reference
Prawn shells	carbon dots (CDs)	9	47
Fingernail	CDs	42.8	48
Lotus root	CDs	19	49
Orange peels	CDs	36	50
Platanus waste	CDs	32	51
Rice husk biomass	GQDs	8	52
Spent tea	GQDs	23	53
Dead neem leaves	GQDs	2	54
Used coffee beans	GQDs	24	55
Waste tonner	GOQDs	10.6	56
Waste diesel-soot	Nonaqueous onion like nanocarbons	6	57
Citrus limon Peel	CQDs	49.5	58
palm kernel shells	CQDs	2.4	59
diesel engine soot	CDs	3	45
diesel engine soot	CDs	1.9	60
kerosene fuel soot	CDs	3	61
Candle soot	CDs	0.8−1.9	62
Petroleum soot	GOQDs	50	this work

The stability of the fluorescence under different pH and temperature conditions was observed, and the results are presented in Figure 3a,b. When the fluorescence intensity of the synthesized GOQDs was investigated at various pH values, it was found that the fluorescence intensity was highest at pH 7.

A significant number of ampholyte groups, including −COOH and −OH (phenolic), attach to the surface of GOQDs, which are very sensitive to pH and have variable isoelectric points and dissociation constants.[63] Thus, it is reasonable to anticipate pH-dependent emission behavior. From these results, it can be said that as the pH increased from 1 to 7, the fluorescence intensity also increased and reached its maximum at pH 7; however, when the pH was further increased from 7 to 11, the fluorescence intensity decreased. However, the fluorescence intensity was affected when the temperature was varied. As the temperature was elevated from 30 to 50 °C, the fluorescence intensity demonstrated a concurrent increase. Similar results were obtained by Wang et al. for carbon dots.[64] In another study, Li et al.,[65] designed the synthesis of graphene quantum dots (GQDs) at various temperature and found that PL intensity decreases with increasing temperature. They claim that a common feature of

https://doi.org/10.1021/acsomega.5c00229
ACS Omega 2025, 10, 14229−14240

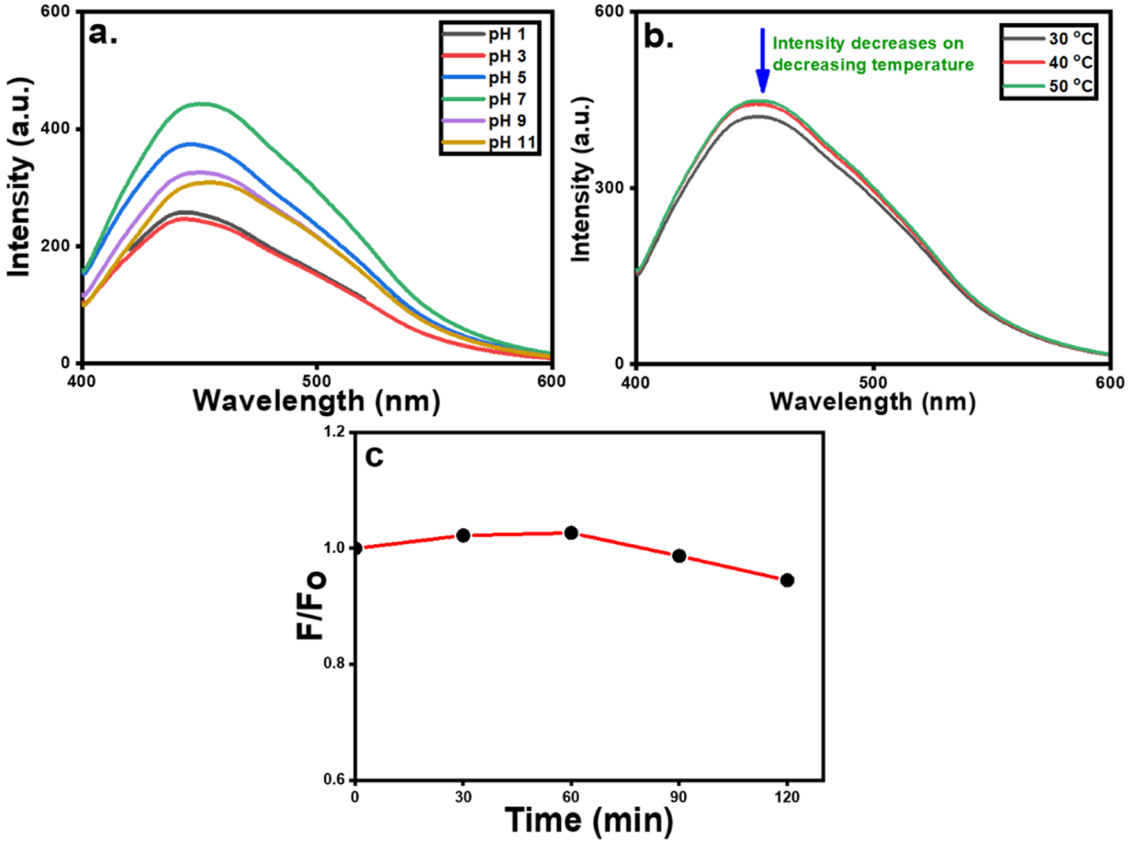

Figure 3. Variation in fluorescence intensity with (a) pH, (b) temperature, and (c) irradiation (by 365 nm UV light).

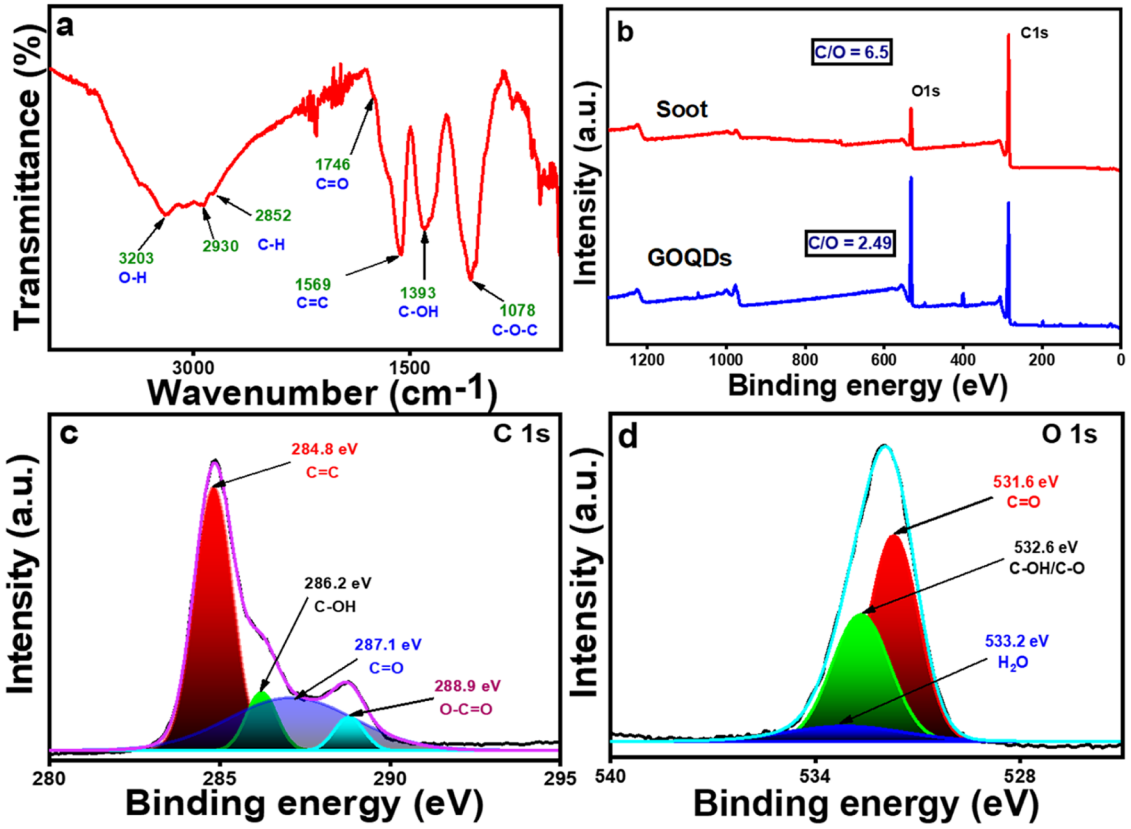

Figure 4. (a) FTIR spectra, (b) XPS spectra of motorcycle exhaust soot (upper one), and GOQDs (lower one); (c, d) are high resolution C 1s and O 1s spectra of exhaust soot-derived GOQDs.

https://doi.org/10.1021/acsomega.5c00229
ACS Omega 2025, 10, 14229−14240

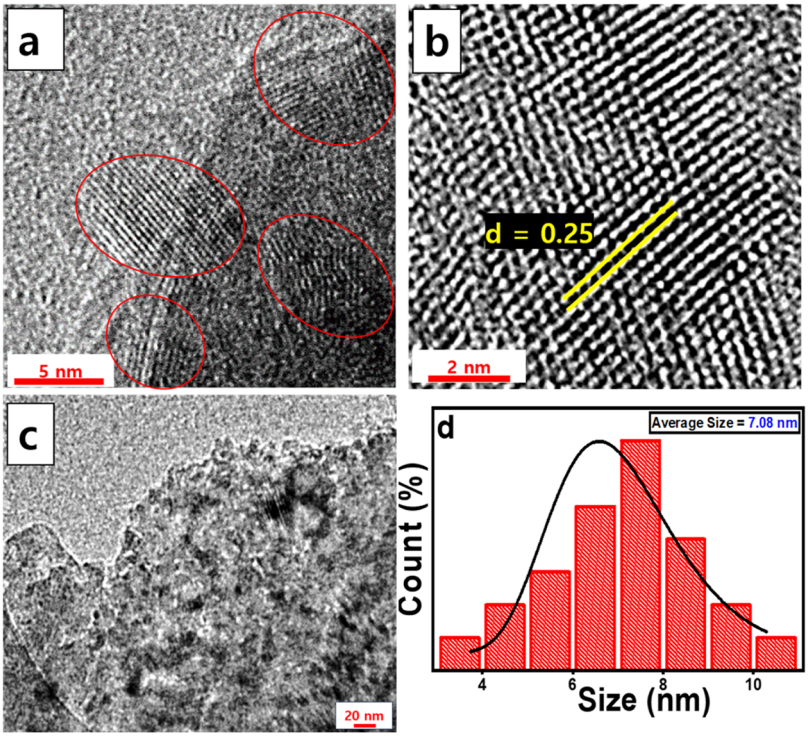

Figure 5. (a) Multilayer, (b) Single layer, and (c) Lattice fringes in HRTEM images under resolution of 5 nm. (d) Area chosen from a HRTEM image (under 50 nm resolution) for size analysis, and (e) corresponding histogram for the GOQDs.

the PL signal of many QDs is the red shift or Stokes shift, which is a result of increasing temperature and occurs due to the nonradiative decay to the lowest vibrational energy level of the excited state. The thermally induced volumetric displacement of lattices, or the equilibrium spacing of atoms, may alter the photon energy exchange during fluorescence excitation as a result of temperature increase, altering the photon energy of the excited fluorescence signal. The photostability of the synthesized GOQDs was evaluated by continuously irradiating the GOQDs in water with UV irradiation (365 nm, 8 W) for 120 min, and the PL intensity was measured; the results are shown in Figure 3c. The normalized PL intensity was >94% even after 120 min i.e., remains almost constant inducing the excellent photostability of prepared GOQDs.[66,67] We also observed the fluorescence of GOQDs treated to HeLa cells using confocal microscopy. The same localization of cells was repeatedly observed at 2 min time intervals, demonstrating that the fluorescence intensity was maintained even after 10 laser scans by confocal microscopy (Figure S1). Therefore, photobleaching of GOQDs does not occur, and GOQDs exhibit excellent photostability for imaging purposes.

3.2.2. Structural Analysis. For structural analysis, the FTIR and XPS results were investigated. In the FTIR spectra (Figure 4a), the aromatic C═C stretching vibration corresponded to strong bands at approximately 1569 cm^{-1}.[68] The C−H bond exhibited stretching frequencies of 2930 and 2852 cm^{-1}.[69] The presence of the −OH, C═O, C−OH, and C−O groups is shown by the clear characteristic peaks at 3203, 1746, 1393, and 1087 cm^{-1}, respectively.[70] The hydrophilic groups can keep the GOQDs stable in an aqueous solution, and these oxygen functional groups are typical of the oxidized forms of graphene (i.e., the GOQDs were generated). All stretching frequencies matched well with those reported in the literature for graphene oxide (GO); hence, it can be concluded that the synthesized material had a GO-like structure.

The produced GOQDs were subjected to elemental analysis using XPS spectroscopy, and the obtained C/O ratio was 2.49, which is similar to the reported C/O ratio (=3 to 1) of graphene oxide (GO).[71] Whereas, the exhaust soot carbon had a C/O ratio of 6.5. Hence, from Figure 4b, it can be clearly seen that a large amount of oxygen was introduced during the oxidation of soot carbon when treated with H_2O_2. Peak at 283−290 eV corresponds to the C 1s peak, whereas for the O 1s spectra, a 530−535 eV range of peak was observed (Figure 4b). By analyzing the C 1s spectra, the following bonds were identified: C═C (284.8 eV), C−OH (286.2 eV), C═O (287.1 eV), and O−C═O (288.9 eV).[72,73] Through analysis of the O 1s spectra, three distinct peak regions were identified at 531.6, 532.6, and 533.2 eV, which correspond to C═O, C−OH (or C−O), and H_2O, respectively.[74] Overall, these results suggest that the sheet-like compound is actually composed of very small-sized graphene oxide quantum dots (GOQDs), which are commonly referred to as GO.

3.2.3. Morphology Analysis. For morphological analysis, HRTEM was performed and the lattice parameter (*d*-spacing) was measured. The lattice fringes are shown in Figure 5d. According to HRTEM analysis, the average size of the GOQDs was 7.08 nm. A histogram of the size analysis is shown in Figure 5d.

The existence of a lattice structure in the GOQDs was revealed by high-resolution transmission electron microscopy (HRTEM) (Figure 5a,b). The lattice spacing was determined to be 0.250 nm, which corresponds to the (1120) plane.[75] A multilayer structure is obtained, as shown in Figure 5a, and a planar sheet-like structure is shown in Figure 5c.

3.3. Application as PL Sensor. The linearity of the chemosensing process was assessed by examining how the

https://doi.org/10.1021/acsomega.5c00229
ACS Omega 2025, 10, 14229−14240

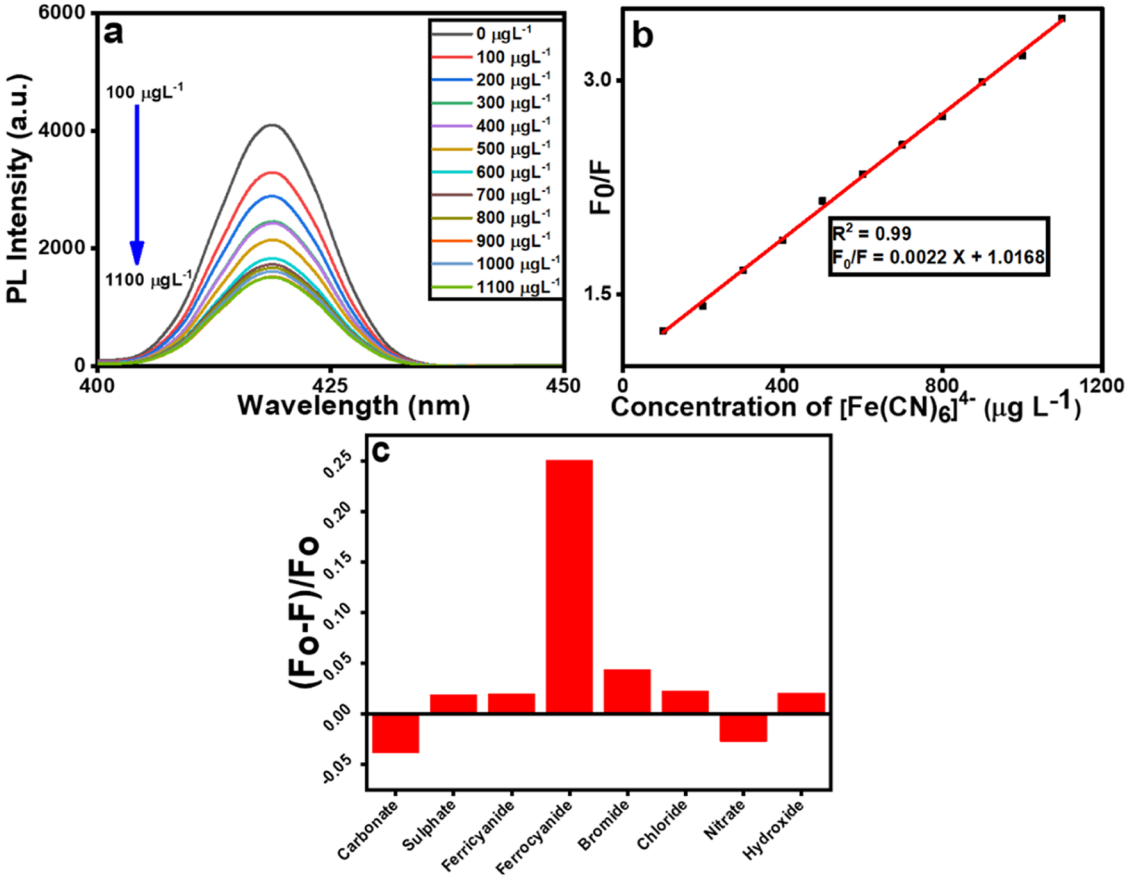

Figure 6. (a) Decreasing fluorescence intensity with increasing concentration of the $[Fe(CN)_6]^{4-}$ ion-containing solution. (b) Relative fluorescence intensity calibration curve as a function of $[Fe(CN)_6]^{4-}$ concentration (Stern−Volmer plot) at ambient temperature. (c) Selectivity study of GOQDs for sensing various anions (100 μmol).

fluorescence intensity of the GOQDs' solution changed upon addition of various amounts of $[Fe(CN)_6]^{4-}$. Figure 6a shows that increasing the concentration of $[Fe(CN)6]^{4-}$ reduced the fluorescence intensity of the GOQDs, indicating the effective quenching ability of $[Fe(CN)6]^{4-}$. To assess the linearity of this sensing system for $[Fe(CN)_6]^{4-}$, the F_0/F ratio was plotted against the $[Fe(CN)_6]^{4-}$ concentration (where F_0 and F are the fluorescence intensities before and after interaction with ferrocyanide). A linear relationship was observed in the concentration range of 100−1100 μg L^{-1} or 100−1100 ng mL^{-1} (Figure 6b), following the Stern−Volmer eq (eq 4)

$$\frac{F_0}{F} = mx + 1 \tag{4}$$

where x is the concentration of $[Fe(CN)_6]^{4-}$ and m denotes the slope of the calibration curve. The linear relationship shown in Figure 6b, is $\frac{F_0}{F} = 0.0022x + 1.0168$. The computed detection limit ($3 \times SD_i/m$, $n = 11$) is 169.05 μg L^{-1} or169.05 ng mL^{-1} or 0.46 nmol mL^{-1}. It is determined that the limits of quantity ($10 \times SD_i/m$, $n = 11$) are 563.5 μg L^{-1} or 563.5 ng mL^{-1} or 1.53 nmol mL^{-1}. The standard deviation of the intercept was calculated from the standard error of the calibration curve using eq 5. The linearity and sensitivity of the proposed fluorescence method were similar to those of previously reported analytical methods.[38] As shown in Table 3, the proposed fluorescence method achieved a considerably higher sensitivity and wider linear range than previously reported results. The proposed fluorescence approach offers the clear benefits of tremendous simplicity, quick analysis, ease of application, and low cost, which undoubtedly open new possibilities for the effective sensing of $[Fe(CN)_6]^{4-}$ ions.

Table 3. Comparison of LOD's of $[Fe(CN)_6]^{4-}$ Ions for Various Sensing Probes

sensors	LOD values	references
N, S, Cl-CNPs	3.3 and 21.8 ng mL^{-1}	38
amine functionalized silica on gold	0.53 nmol mL^{-1}	76
spectroelectrochemical sensor	50 nmol mL^{-1}	77
motorcycle soot derived GOQDs	0.46 nmol mL^{-1}	this work

$$SD_i = SE \times n^{1/2} \tag{5}$$

To study the selectivity of the GOQDs sensor for $[Fe(CN)_6]^{4-}$ detection, the intensity ratios of F/F_0 for the GOQDs in the presence of various anions, including ferricyanide ($[Fe(CN)_6]^{3-}$), chloride (Cl^-), bromide (Br^-), hydroxide (OH^-), nitrate (NO_3^-), carbonate (CO_3^{2-}), and sulfate (SO_4^{2-}), were obtained, as shown in Figure 6c. The concentration of each anion, including $[Fe(CN)_6]^{4-}$, was 100 μM. The addition of $[Fe(CN)_6]^{4-}$ to the GOQDs solution resulted in an apparent decrease in the fluorescence intensity, whereas the remaining anions exerted no effect under the same optimal conditions.[78]

To study the sensing mechanism for $[Fe(CN)_6]^{4-}$ detection, the absorption spectrum of $[Fe(CN)_6]^{4-}$ and the excitation and emission spectra of GOQDs were compared. The

https://doi.org/10.1021/acsomega.5c00229
ACS Omega 2025, 10, 14229−14240

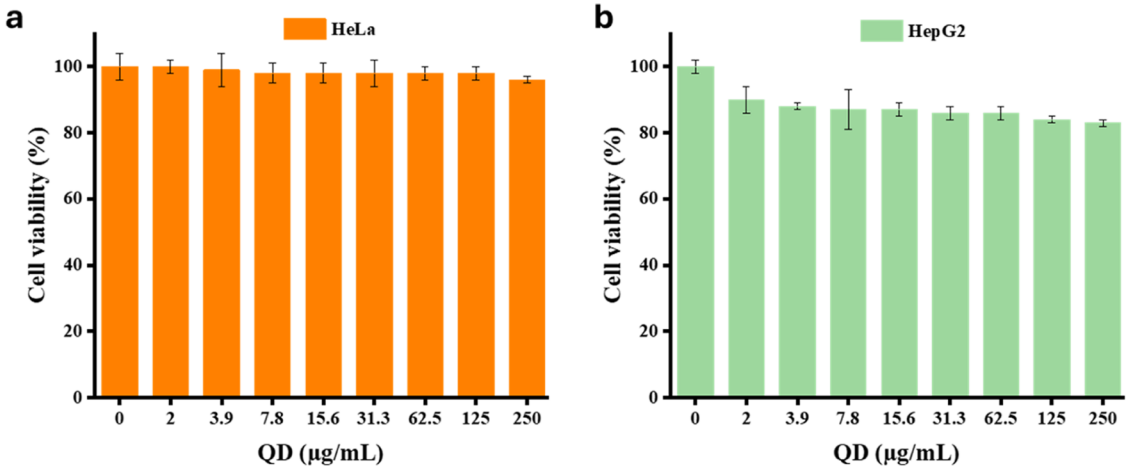

Figure 7. Cell viability data for (a). HeLa and (b) HepG2 cells treated with various concentrations of GOQDs.

excitation spectrum of the GOQDs shows an excitation peak at 320 nm, and $[Fe(CN)_6]^{4-}$ exhibits two absorption bands at 269 and 326 nm, respectively;[38] hence, a good overlap between the excitation spectrum of the GOQDs and the absorbance of $[Fe(CN)_6]^{4-}$ can be concluded. Thus, it can concluded that the sensing mechanism is primary inner filter effect (PIFE). No overlap was observed between the absorption spectrum of $[Fe(CN)_6]^{4-}$ and the emission spectrum of the GOQDs (Figure 2a). Therefore, the interaction between the GOQDs and $[Fe(CN)_6]^{4-}$ does not result from Förster resonant energy transfer (FRET) or the secondary inner filter effect (SIFE).[79]

3.4. Cytotoxicity of GOQDs. The produced water-dispersible GOQDs exhibited potential for use in biological applications. To determine whether GOQDs could be used as bioprobes, the toxicity and viability of HeLa and HepG2 cells after treatment with various concentrations of GOQDs were investigated. After 24 h of incubation, the cells were analyzed using the MTT assay to determine cell viability. As shown in Figure 7a,b, HeLa cells exhibited cell viability exceeding 96% at the maximum concentration, while HepG2 cells maintained viability above 83%, indicating that the GOQDs possess low cytotoxicity toward both cell lines. Conventional QDs are known to be highly toxic to humans because of the presence of heavy metals such as cadmium. In contrast, GOQDs are not as harmful as conventional QDs, implying that they could be useful bioimaging tools in biological studies that require photostable, bright, harmless, and cell-permeable agents.

3.5. Bioimaging of GOQDs. The cellular uptake of GOQDs in live HeLa cells was examined using confocal microscopy. Cells were treated with 10 μM GOQDs for different incubation times. We found that an incubation time of at least 4 h was required for the GOQDs to be sufficiently internalized into the cells and to observe the blue fluorescence emitted by the GOQDs. Thus, a 4 h incubation time was fixed throughout the rest of the study. After 4 h of incubation of the GOQDs in HeLa cells, the cells were washed three times with cell medium to remove any noninternalized GOQDs. The cells were then treated with DRAQ5 (10 μM) which is a specific marker of cell nuclei that emits red fluorescence. The GOQDs were predominantly localized in the cytoplasm but not in the cell nucleus, possibly because of their size (Figure 8a). To confirm the cellular localization of GOQDs, GOQD-treated cells were incubated again with another marker, Mito Tracker (100 nM), which specifically stains mitochondria with red

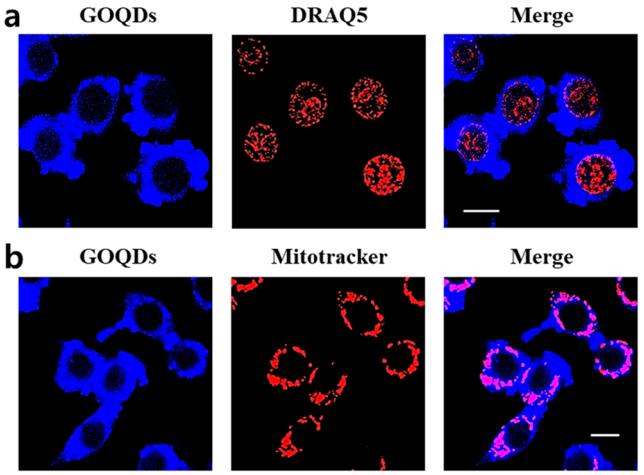

Figure 8. Cellular uptake of GOQDs (10 μM, 4 h incubation) by HeLa cells was observed using confocal microscopy. (a) HeLa cells incubated with GOQDs (blue), DRAQ5 (red), and merged image (right third), (b) HeLa cells incubated with GOQDs (blue), or MitoTracker (red), and the merge image (right third), scale bar: 10 μm.

fluorescence. We observed that the GOQDs colocalized with the Mito Tracker in the merged image (Figure 8b). Mitochondria exist only in the cytoplasm, and the observations above show that GOQDs do not enter the nucleus but diffuse only into the cytoplasm, including the mitochondria. It has been previously reported that conventional QDs do not internalize into HeLa cells and that they need to undergo surface modification to increase the cell membrane permeability. Interestingly, the GOQDs were well taken up by HeLa cells even without any chemical modification of the particle surface. This suggests that GOQDs are a promising bioimaging tool for cancer treatment.

4. CONCLUSIONS

This study demonstrates the synthesis of motorcycle soot-derived GOQDs, which are used for chemo- and biosensing applications. The GOQDs were characterized using several techniques such as UV−vis spectroscopy, PL spectroscopy, XPS, FTIR, and HRTEM. From the UV−vis spectra, the GOQDs exhibited $\pi-\pi^*$ transitions of aromatic C═C and $n-\pi^*$ transitions of C═O. Under 365 nm UV light, a strong

https://doi.org/10.1021/acsomega.5c00229
ACS Omega 2025, 10, 14229−14240

blue-emissive light was observed. The QY was also calculated for the synthesized GOQDs and found to be approximately 50% relative to that of quinine sulfate (QY = 54.6%). In the XPS spectra, the C/O ratio is 2.49, which is closer to that of GO. By analyzing the C 1s and O 1s spectra, the following bonds were identified: C═C, C−OH, C═O O−C═O, and C−O. Lattice fringes are clearly visible in the HRTEM images of the GOQDs; the average size of the GOQDs was 7.3 nm in average. Chemosensing experiments showed that, as the ferrocyanide concentration increased, the fluorescence intensity of the GOQDs decreased. The chemosensing of ferrocyanide ion revealed that the LOD value was 0.46 nmol mL^{-1} which was quite better value compared to the reported literature. The sensing mechanism involved was PIFE. While conducting the bioimaging test (using Mitotracker and nucleus tracker), it was found that the GOQDs could be spread over the entire cell, except for the nucleus, probably because of the size effect. As the GOQDs were not very toxic to HeLa and HepG2 cell lines, they could be efficiently used for the detection of cancer cells.

■ ASSOCIATED CONTENT

Data Availability Statement

The data sets used and/or analyzed during the current study are available from the corresponding author upon reasonable request.

Supporting Information

The Supporting Information is available free of charge at https://pubs.acs.org/doi/10.1021/acsomega.5c00229.

> HeLa cells were treated with GOQDs, and were observed with confocal microscopy repeatedly with time intervals. The fluorescence does not diminish (Figure S1) (PDF)

■ AUTHOR INFORMATION

Corresponding Authors

Jungkyun Im − *Department of Electronic Materials, Devices, and Equipment Engineering, Soonchunhyang University, Asan 31538, Republic of Korea; Department of Chemical Engineering, Soonchunhyang University, Asan 31538, Republic of Korea;* orcid.org/0000-0002-7926-5815; Email: jkim5279@sch.ac.kr

Goutam Biswas − *Department of Chemistry, Cooch Behar Panchanan Barma University, Cooch Behar 736101, India;* orcid.org/0000-0002-1488-2003; Email: goutam@cbpbu.ac.in

Authors

Chanchal Das − *Department of Chemistry, Cooch Behar Panchanan Barma University, Cooch Behar 736101, India*

Nasim Sepay − *Department of Electronic Materials, Devices, and Equipment Engineering, Soonchunhyang University, Asan 31538, Republic of Korea*

Tae Wan Kim − *Department of Medical Life Science, Soonchunhyang University, Asan 31538, Republic of Korea*

Shinwon Chae − *Department of Biochemistry, Soonchunhyang University, College of Medicine, Cheonan 31151, Republic of Korea*

Nandan Ghosh − *Department of Electronic Materials, Devices, and Equipment Engineering, Soonchunhyang University, Asan 31538, Republic of Korea*

Mohan Dumpala − *Department of Electronic Materials, Devices, and Equipment Engineering, Soonchunhyang University, Asan 31538, Republic of Korea*

Dongsic Choi − *Department of Biochemistry, Soonchunhyang University, College of Medicine, Cheonan 31151, Republic of Korea;* orcid.org/0000-0002-2516-5616

Seob Jeon − *Department of Obstetrics and Gynecology, College of Medicine, Soonchunhyang University Cheonan Hospital, Cheonan 31151, Republic of Korea*

Complete contact information is available at: https://pubs.acs.org/10.1021/acsomega.5c00229

Author Contributions

Conceptualization, methodology, formal analysis, investigation, and writing the original draft: C.D., G.B., J.I.; Formal analysis, writing, and review: N.S., T.W.K., S.C., N.G., M.D., D.C., S.J.; Supervision: J.I. and G.B.; Writing − review and editing, J.I., D.C., and G.B.

Funding

This work was funded by BK21 FOUR (Fostering Outstanding Universities for Research) (No. 5199991614564) and the Soonchunhyang University Research Fund.

Notes

The authors declare no competing financial interest.

■ ACKNOWLEDGMENTS

This work was funded by BK21 FOUR (Fostering Outstanding Universities for Research) (No.: 5199991614564) and by the Soonchunhyang University Research Fund.

■ REFERENCES

(1) Abdel-Shafy, H. I.; Mansour, M. S. M. Solid Waste Issue: Sources, Composition, Disposal, Recycling, and Valorization. *Egypt. J. Pet.* **2018**, *27* (4), 1275−1290.

(2) Chien, C.-F.; Aviso, K.; Tseng, M.-L.; Fujii, M.; Lim, M. K. Solid Waste Management in Emerging Economies: Opportunities and Challenges for Reuse and Recycling. *Resour. Conserv. Recycl.* **2021**, *172*, No. 105677.

(3) Wang, Q.; Liu, X.; Zhang, L.; Lv, Y. Microwave-Assisted Synthesis of Carbon Nanodots through an Eggshell Membrane and Their Fluorescent Application. *Analyst* **2012**, *137* (22), 5392.

(4) Pandiyan, S.; Arumugam, L.; Srirengan, S. P.; Pitchan, R.; Sevugan, P.; Kannan, K.; Pitchan, G.; Hegde, T. A.; Gandhirajan, V. Biocompatible Carbon Quantum Dots Derived from Sugarcane Industrial Wastes for Effective Nonlinear Optical Behavior and Antimicrobial Activity Applications. *ACS Omega* **2020**, *5* (47), 30363−30372.

(5) Zhou, J.; Sheng, Z.; Han, H.; Zou, M.; Li, C. Facile Synthesis of Fluorescent Carbon Dots Using Watermelon Peel as a Carbon Source. *Mater. Lett.* **2012**, *66* (1), 222−224.

(6) Sharma, R.; Sharma, A.; Chen, C. Emerging Trends of Nanotechnology towards Picotechnology: Energy and Biomolecules. *Nat. Preced.* **2011**, 1-1 DOI: 10.1038/npre.2010.4525.1.

(7) Huang, C.; Chen, C.; Zhang, M.; Lin, L.; Ye, X.; Lin, S.; Antonietti, M.; Wang, X. Carbon-Doped BN Nanosheets for Metal-Free Photoredox Catalysis. *Nat. Commun.* **2015**, *6* (1), No. 7698.

(8) Pulizzi, F. Nanotechnology in Food: Silver-Lined Packaging. *Nat. Nanotechnol.* **2016**, 1-1 DOI: 10.1038/nnano.2016.11.

(9) Das, C.; Nath Ghosh, N.; Bhardwaj, R.; Narula, K.; Mishra, P.; Biswas, G. Enhanced Photocatalytic Degradation of a Hydrocortisone by Biomodified and Biocompatible Magnetite Nanoparticles and Its Mechanistic Assessment. *J. Ind. Eng. Chem.* **2023**, *128*, 369−382.

(10) Shi, X.; Zhang, X.; Gao, W.; Zhang, Y.; He, D. Removal of Microplastics from Water by Magnetic Nano-Fe3O4. *Sci. Total Environ.* **2022**, *802*, No. 149838.

(11) Das, C.; Ghosh, N. N.; Pulhani, V.; Biswas, G.; Singhal, P. Bio-Functionalized Magnetic Nanoparticles for Cost-Effective Adsorption of U(VI): Experimental and Theoretical Investigation. *RSC Adv.* **2023**, *13* (22), 15015−15023.
(12) Das, C.; Sillanpää, M.; Zaidi, S. A.; Khan, M. A.; Biswas, G. Current Trends in Carbon-Based Quantum Dots Development from Solid Wastes and Their Applications. *Environ. Sci. Pollut. Res.* **2023**, *30* (16), 45528−45554.
(13) Das, C.; Singh, S.; Bhakta, S.; Mishra, P.; Biswas, G. Bio-Modified Magnetic Nanoparticles with Terminalia Arjuna Bark Extract for the Removal of Methylene Blue and Lead (II) from Simulated Wastewater. *Chemosphere* **2022**, *291*, No. 132673.
(14) Das, C.; Sen, S.; Singh, T.; Ghosh, T.; Paul, S. S.; Kim, T. W.; Jeon, S.; Maiti, D. K.; Im, J.; Biswas, G. Green Synthesis, Characterization and Application of Natural Product Coated Magnetite Nanoparticles for Wastewater Treatment. *Nanomaterials* **2020**, *10* (8), 1615.
(15) Ghosh, N.; Sen, S.; Biswas, G.; Saxena, A.; Haldar, P. K. Adsorption and Desorption Study of Reusable Magnetic Iron Oxide Nanoparticles Modified with Justicia Adhatoda Leaf Extract for the Removal of Textile Dye and Antibiotic. *Water, Air, Soil Pollut.* **2023**, *234* (3), 202.
(16) El Hachmi, A.; Sen, S.; Mondal, R.; Paul, M.; Saha, A.; Im, J.; Biswas, G. Structural, Morphological, Magnetic and Optical Properties of Jeanbandyite Prepared by the Co-Precipitation Method. *Mater. Today Commun.* **2023**, *34*, No. 105358.
(17) Ghosh, N.; Sen, S.; Biswas, G.; Singh, L. R.; Chakdar, D.; Haldar, P. K. A Comparative Study of CuO Nanoparticle and CuO/PVA-PVP Nanocomposite on the Basis of Dye Removal Performance and Antibacterial Activity in Wastewater Treatment. *Int. J. Environ. Anal. Chem.* **2022**, 1−21.
(18) Bayda, S.; Adeel, M.; Tuccinardi, T.; Cordani, M.; Rizzolio, F. The History of Nanoscience and Nanotechnology: From Chemical−Physical Applications to Nanomedicine. *Molecules* **2020**, *25* (1), 112.
(19) Ahmadi, S.; Ebrahimi Warkiani, M.; Rabiee, M.; Iravani, S.; Rabiee, N. Carbon-Based Nanomaterials against SARS-CoV-2: Therapeutic and Diagnostic Applications. *OpenNano* **2023**, *10*, No. 100121.
(20) Koepfli, S. M.; Baumann, M.; Koyaz, Y.; Gadola, R.; Güngör, A.; Keller, K.; Horst, Y.; Nashashibi, S.; Schwanninger, R.; Doderer, M.; Passerini, E.; Fedoryshyn, Y.; Leuthold, J. Metamaterial Graphene Photodetector with Bandwidth Exceeding 500 Gigahertz. *Science* **2023**, *380* (6650), 1169−1174.
(21) Kong, W.; Kum, H.; Bae, S.-H.; Shim, J.; Kim, H.; Kong, L.; Meng, Y.; Wang, K.; Kim, C.; Kim, J. Path towards Graphene Commercialization from Lab to Market. *Nat. Nanotechnol.* **2019**, *14* (10), 927−938.
(22) Akinwande, D.; Huyghebaert, C.; Wang, C.-H.; Serna, M. I.; Goossens, S.; Li, L.-J.; Wong, H.-S. P.; Koppens, F. H. L. Graphene and Two-Dimensional Materials for Silicon Technology. *Nature* **2019**, *573* (7775), 507−518.
(23) Bairi, P.; Minami, K.; Nakanishi, W.; Hill, J. P.; Ariga, K.; Shrestha, L. K. Hierarchically Structured Fullerene C 70 Cube for Sensing Volatile Aromatic Solvent Vapors. *ACS Nano* **2016**, *10* (7), 6631−6637.
(24) Luo, S.; Chen, X.; He, Y.; Gu, Y.; Zhu, C.; Yang, G.-H.; Qu, L.-L. Recent Advances in Graphene Nanoribbons for Biosensing and Biomedicine. *J. Mater. Chem. B* **2021**, *9* (31), 6129−6143.
(25) Akin, M.; Bekmezci, M.; Bayat, R.; Coguplugil, Z. K.; Sen, F.; Karimi, F.; Karimi-Maleh, H. Mobile Device Integrated Graphene Oxide Quantum Dots Based Electrochemical Biosensor Design for Detection of MiR-141 as a Pancreatic Cancer Biomarker. *Electrochim. Acta* **2022**, *435*, No. 141390.
(26) Ji, S.-r.; Liu, C.; Zhang, B.; Yang, F.; Xu, J.; Long, J.; Jin, C.; Fu, D.; Ni, Q.; Yu, X. Carbon Nanotubes in Cancer Diagnosis and Therapy. *Biochim. Biophys. Acta - Rev. Cancer* **2010**, *1806* (1), 29−35.
(27) Mohammed-Ahmed, H. K.; Nakipoglu, M.; Tezcaner, A.; Keskin, D.; Evis, Z. Functionalization of Graphene Oxide Quantum Dots for Anticancer Drug Delivery. *J. Drug Delivery Sci. Technol.* **2023**, *80*, No. 104199.
(28) Aksoy, B. T.; Çoşut, B. Graphene/Graphene Oxide−Based Nanomaterials for Hydrogen Production and Storage Applications. In *Nanomaterials for Hydrogen Storage Applications*; Elsevier, 2021; pp 97−116.
(29) Tsai, K.-A.; Hsieh, P.-Y.; Lai, T.-H.; Tsao, C.-W.; Pan, H.; Lin, Y.-G.; Hsu, Y.-J. Nitrogen-Doped Graphene Quantum Dots for Remarkable Solar Hydrogen Production. *ACS Appl. Energy Mater.* **2020**, *3* (6), 5322−5332.
(30) Wang, T.; Zhang, L.; Wu, J.; Chen, M.; Yang, S.; Lu, Y.; Du, P. Few-Layer Fullerene Network for Photocatalytic Pure Water Splitting into H2 and H2O2. *Angew. Chem., Int. Ed.* **2023**, *62* (40), e202311352 DOI: 10.1002/anie.202311352.
(31) Miao, L.; Song, Z.; Zhu, D.; Li, L.; Gan, L.; Liu, M. Recent Advances in Carbon-Based Supercapacitors. *Mater. Adv.* **2020**, *1* (5), 945−966.
(32) Debnath, S. K.; Srivastava, R. Drug Delivery With Carbon-Based Nanomaterials as Versatile Nanocarriers: Progress and Prospects. *Front. Nanotechnol.* **2021**, *3*, 644564 DOI: 10.3389/fnano.2021.644564.
(33) Lin, J.; Chen, L.; Jiang, W.; Zhang, H.; Shi, Y.; Cai, W. Rapid Detection of Low-level HeLa Cell Contamination in Cell Culture Using Nested PCR. *J. Cell. Mol. Med.* **2019**, *23* (1), 227−236.
(34) Soleymani, J.; Azizi, S.; Abbaspour-Ravasjani, S.; Hasanzadeh, M.; Hossein Somi, M.; Jouyban, A. Glycoprotein-Based Bioimaging of HeLa Cancer Cells by Folate Receptor and Folate Decorated Graphene Quantum Dots. *Microchem. J.* **2021**, *170*, No. 106732.
(35) Du, Y.; Li, Y.; Liu, Y.; Liu, N.; Cheng, Y.; Shi, Q.; Liu, X.; Tao, Z.; Guo, Y.; Zhang, J.; Askaria, N.; Li, H. Stalk-Derived Carbon Dots as Nanosensors for Fe3+ Ions Detection and Biological Cell Imaging. *Front. Bioeng. Biotechnol.* **2023**, *11*, 1187632 DOI: 10.3389/fbioe.2023.1187632.
(36) Nagaraj, M.; Ramalingam, S.; Murugan, C.; Aldawood, S.; Jin, J.-O.; Choi, I.; Kim, M. Detection of Fe3+ Ions in Aqueous Environment Using Fluorescent Carbon Quantum Dots Synthesized from Endosperm of Borassus Flabellifer. *Environ. Res.* **2022**, *212*, No. 113273.
(37) Tshangana, C. S.; Muleja, A. A.; Kuvarega, A. T.; Malefetse, T. J.; Mamba, B. B. The Applications of Graphene Oxide Quantum Dots in the Removal of Emerging Pollutants in Water: An Overview. *J. Water Process Eng.* **2021**, *43*, No. 102249.
(38) Hu, Q.; Pan, Y.; Gong, X.; Rao, S.; Xiao, L.; Liu, L.; Yang, Z. A Sensitivity Enhanced Fluorescence Method for the Detection of Ferrocyanide Ions in Foodstuffs Using Carbon Nanoparticles as Sensing Agents. *Food Chem.* **2020**, *308*, No. 125590.
(39) Na, M.; Chen, Y.; Han, Y.; Ma, S.; Liu, J.; Chen, X. Determination of Potassium Ferrocyanide in Table Salt and Salted Food Using a Water-Soluble Fluorescent Silicon Quantum Dots. *Food Chem.* **2019**, *288*, 248−255.
(40) Ding, H.; Yu, S.-B.; Wei, J.-S.; Xiong, H.-M. Full-Color Light-Emitting Carbon Dots with a Surface-State-Controlled Luminescence Mechanism. *ACS Nano* **2016**, *10* (1), 484−491.
(41) Kim, S.; Hwang, S. W.; Kim, M.-K.; Shin, D. Y.; Shin, D. H.; Kim, C. O.; Yang, S. B.; Park, J. H.; Hwang, E.; Choi, S.-H.; Ko, G.; Sim, S.; Sone, C.; Choi, H. J.; Bae, S.; Hong, B. H. Anomalous Behaviors of Visible Luminescence from Graphene Quantum Dots: Interplay between Size and Shape. *ACS Nano* **2012**, *6* (9), 8203−8208.
(42) Nugroho, B. S.; Nakashima, S. Improvement of Cs Detection Performance and Formation of CsCl and Cs Nanoparticles by Tuning Graphene Oxide Quantum Dot-Based Nanocomposite. *RSC Adv.* **2022**, *12* (30), 19667−19677.
(43) Sawalha, S.; Assali, M.; Yaseen, A.; Ataya, A.; Refai, L.; Hamed, R.; Misia, G.; Collavini, S.; Silvestri, A. Carbon Nanodots Synthesized from Used Tobacco Molasses as Promising Selective Probes for Fe (III) Ion Sensing. *Mater. Today Sustain.* **2024**, *25*, No. 100697.

(44) Mondal, M.; Pramanik, S. A Mechanism for Excitation-Dependent Emission from Carbon Nanodots. *Mater. Lett. X* **2023**, *18*, No. 100195.
(45) Thulasi, S.; Kathiravan, A.; Asha Jhonsi, M. Fluorescent Carbon Dots Derived from Vehicle Exhaust Soot and Sensing of Tartrazine in Soft Drinks. *ACS Omega* **2020**, *5* (12), 7025−7031.
(46) Issa, M. A.; Abidin, Z. Z.; Sobri, S.; Rashid, S. A.; Mahdi, M. A.; Ibrahim, N. A. Fluorescent Recognition of Fe3+ in Acidic Environment by Enhanced-Quantum Yield N-Doped Carbon Dots: Optimization of Variables Using Central Composite Design. *Sci. Rep.* **2020**, *10* (1), No. 11710.
(47) Gedda, G.; Lee, C.-Y.; Lin, Y.-C.; Wu, H. Green Synthesis of Carbon Dots from Prawn Shells for Highly Selective and Sensitive Detection of Copper Ions. *Sensors Actuators B Chem.* **2016**, *224*, 396−403.
(48) Chatzimitakos, T.; Kasouni, A.; Sygellou, L.; Leonardos, I.; Troganis, A.; Stalikas, C. Human Fingernails as an Intriguing Precursor for the Synthesis of Nitrogen and Sulfur-Doped Carbon Dots with Strong Fluorescent Properties: Analytical and Bioimaging Applications. *Sensors Actuators B Chem.* **2018**, *267*, 494−501.
(49) Gu, D.; Shang, S.; Yu, Q.; Shen, J. Green Synthesis of Nitrogen-Doped Carbon Dots from Lotus Root for Hg(II) Ions Detection and Cell Imaging. *Appl. Surf. Sci.* **2016**, *390*, 38−42.
(50) Prasannan, A.; Imae, T. One-Pot Synthesis of Fluorescent Carbon Dots from Orange Waste Peels. *Ind. Eng. Chem. Res.* **2013**, *52* (44), 15673−15678.
(51) Ren, X.; Zhang, F.; Guo, B.; Gao, N.; Zhang, X. Synthesis of N-Doped Micropore Carbon Quantum Dots with High Quantum Yield and Dual-Wavelength Photoluminescence Emission from Biomass for Cellular Imaging. *Nanomaterials* **2019**, *9* (4), 495.
(52) Wang, Z.; Fu, B.; Zou, S.; Duan, B.; Chang, C.; Yang, B.; Zhou, X.; Zhang, L. Facile Construction of Carbon Dots via Acid Catalytic Hydrothermal Method and Their Application for Target Imaging of Cancer Cells. *Nano Res.* **2016**, *9* (1), 214−223.
(53) Abbas, A.; Tabish, T. A.; Bull, S. J.; Lim, T. M.; Phan, A. N. High Yield Synthesis of Graphene Quantum Dots from Biomass Waste as a Highly Selective Probe for Fe3+ Sensing. *Sci. Rep.* **2020**, *10* (1), No. 21262.
(54) Suryawanshi, A.; Biswal, M.; Mhamane, D.; Gokhale, R.; Patil, S.; Guin, D.; Ogale, S. Large Scale Synthesis of Graphene Quantum Dots (GQDs) from Waste Biomass and Their Use as an Efficient and Selective Photoluminescence on−off−on Probe for Ag + Ions. *Nanoscale* **2014**, *6* (20), 11664−11670.
(55) Wang, S.; Cole, I. S.; Li, Q. The Toxicity of Graphene Quantum Dots. *RSC Adv.* **2016**, *6* (92), 89867−89878.
(56) Xu, Q.; Gong, Y.; Zhang, Z.; Miao, Y.; Li, D.; Yan, G. Preparation of Graphene Oxide Quantum Dots from Waste Toner, and Their Application to a Fluorometric DNA Hybridization Assay. *Microchim. Acta* **2019**, *186* (7), 483.
(57) Gunture, K.; Garg, A. K.; Aggarwal, R.; Kaushik, J.; Prajapati, R. K.; Sonkar, S. K. Non-Aqueous Onion like Nano-Carbons from Waste Diesel-Soot Used as FRET-Based Sensor for Sensing of Nitro-Phenols. *Environ. Res.* **2022**, *212*, No. 113308.
(58) Kundu, A.; Basu, S.; Maity, B. Upcycling Waste: Citrus Limon Peel-Derived Carbon Quantum Dots for Sensitive Detection of Tetracycline in the Nanomolar Range. *ACS Omega* **2023**, *8* (39), 36449−36459.
(59) Abu, N.; Chinnathambi, S.; Kumar, M.; Etezadi, F.; Bakhori, N. M.; Zubir, Z. A.; Md Salleh, S. N.; Shueb, R. H.; Karthikeyan, S.; Thangavel, V.; Abdullah, J.; Pandian, G. N. Development of Biomass Waste-Based Carbon Quantum Dots and Their Potential Application as Non-Toxic Bioimaging Agents. *RSC Adv.* **2023**, *13* (40), 28230−28249.
(60) Tripathi, K. M.; Sonker, A. K.; Sonkar, S. K.; Sarkar, S. Pollutant Soot of Diesel Engine Exhaust Transformed to Carbon Dots for Multicoloured Imaging of *E. Coli* and Sensing Cholesterol. *RSC Adv.* **2014**, *4* (57), 30100.
(61) Venkatesan, S.; Mariadoss, A. J.; Arunkumar, K.; Muthupandian, A. Fuel Waste to Fluorescent Carbon Dots and Its Multifarious Applications. *Sensors Actuators B Chem.* **2019**, *282*, 972−983.
(62) Liu, H.; Ye, T.; Mao, C. Fluorescent Carbon Nanoparticles Derived from Candle Soot. *Angew. Chem., Int. Ed.* **2007**, *46* (34), 6473−6475.
(63) Zou, W.-S.; Kong, W.-L.; Zhao, Q.-C.; Zhang, J.; Zhao, X.; Zhao, D.; Wang, Y.-Q. A Composite Consisting of Bromine-Doped Carbon Dots and Ferric Ions as a Fluorescent Probe for Determination and Intracellular Imaging of Phosphate. *Microchim. Acta* **2019**, *186* (8), 576.
(64) Wang, Q.; Tang, Z.; Li, L.; Guo, J.; Jin, L.; Lu, J.; Huang, P.; Zhang, S.; Jiao, L. Highly Efficient Red-Emitting Carbon Dots as a "Turn-on" Temperature Probe in Living Cells. *Spectrochim. Acta Part A Mol. Biomol. Spectrosc.* **2022**, *280*, No. 121538.
(65) Li, C.; Yue, Y. Fluorescence Spectroscopy of Graphene Quantum Dots: Temperature Effect at Different Excitation Wavelengths. *Nanotechnology* **2014**, *25* (43), No. 435703.
(66) Dua, S.; Kumar, P.; Pani, B.; Kaur, A.; Khanna, M.; Bhatt, G. Stability of Carbon Quantum Dots: A Critical Review. *RSC Adv.* **2023**, *13* (20), 13845−13861.
(67) Guo, Y.; Zhang, L.; Cao, F.; Leng, Y. Thermal Treatment of Hair for the Synthesis of Sustainable Carbon Quantum Dots and the Applications for Sensing Hg2+. *Sci. Rep.* **2016**, *6* (1), No. 35795.
(68) Yan, Q.-L.; Cohen, A.; Petrutik, N.; Shlomovich, A.; Burstein, L.; Pang, S.-P.; Gozin, M. Highly Insensitive and Thermostable Energetic Coordination Nanomaterials Based on Functionalized Graphene Oxides. *J. Mater. Chem. A* **2016**, *4* (25), 9941−9948.
(69) Luceño-Sánchez, J. A.; Maties, G.; Gonzalez-Arellano, C.; Díez-Pascual, A. M. Synthesis and Characterization of Graphene Oxide Derivatives via Functionalization Reaction with Hexamethylene Diisocyanate. In *IOCN 2018*; MDPI: Basel Switzerland, 2018; p 8.
(70) Khalili, D. Graphene Oxide: A Promising Carbocatalyst for the Regioselective Thiocyanation of Aromatic Amines, Phenols, Anisols and Enolizable Ketones by Hydrogen Peroxide/KSCN in Water. *New J. Chem.* **2016**, *40* (3), 2547−2553.
(71) Tiginyanu, I.; Ursaki, V.; Popa, V. Ultra-Thin Membranes for Sensor Applications. In *Nanocoatings and Ultra-Thin Films*; Elsevier, 2011; pp 330−354.
(72) Wang, W.; Lu, Y.-C.; Huang, H.; Wang, A.-J.; Chen, J.-R.; Feng, J.-J. Facile Synthesis of N, S-Codoped Fluorescent Carbon Nanodots for Fluorescent Resonance Energy Transfer Recognition of Methotrexate with High Sensitivity and Selectivity. *Biosens. Bioelectron.* **2015**, *64*, 517−522.
(73) Liu, L.-L.; Liu, L.; Wang, C.-Y.; Zhang, L.; Feng, J.-J.; Gao, Y.-J.; Wang, A.-J. Strong Coupling Fe2VO4 Nanoparticles/3D N-Doped Interconnected Porous Carbon Derived from MOFs by Confined Adsorption-Assembly-Pyrolysis for Greatly Boosting Oxygen Reduction. *J. Colloid Interface Sci.* **2025**, *684*, 10−20.
(74) Zhang, B.; Li, L.; Wang, Z.; Xie, S.; Zhang, Y.; Shen, Y.; Yu, M.; Deng, B.; Huang, Q.; Fan, C.; Li, J. Radiation Induced Reduction: An Effective and Clean Route to Synthesize Functionalized Graphene. *J. Mater. Chem.* **2012**, *22* (16), 7775.
(75) Kang, S.; Kim, K. M.; Jung, K.; Son, Y.; Mhin, S.; Ryu, J. H.; Shim, K. B.; Lee, B.; Han, H.; Song, T. Graphene Oxide Quantum Dots Derived from Coal for Bioimaging: Facile and Green Approach. *Sci. Rep.* **2019**, *9* (1), No. 4101.
(76) Almeida Júnior, P. L.; Mendes, C. H. S.; Lima, I. A. F. S.; Belian, M. F.; Oliveira, S. C. B.; Brett, C. M. A.; Nascimento, V. B. Ferricyanide Confined in a Protonated Amine-Functionalized Silica Film on Gold: Application to Electrocatalytic Sensing of Nitrite Ions. *Anal. Lett.* **2018**, *51* (4), 496−511.
(77) Stegemiller, M. L.; Heineman, W. R.; Seliskar, C. J.; Ridgway, T. H.; Bryan, S. A.; Hubler, T.; Sell, R. L. Spectroelectrochemical Sensing Based on Multimode Selectivity Simultaneously Achievable in a Single Device. 11. Design and Evaluation of a Small Portable Sensor for the Determination of Ferrocyanide in Hanford Waste Samples. *Environ. Sci. Technol.* **2003**, *37* (1), 123−130.
(78) Kongsanan, N.; Pimsin, N.; Keawprom, C.; Sricharoen, P.; Areerob, Y.; Nuengmatcha, P.; Oh, W.-C.; Chanthai, S.;

https://doi.org/10.1021/acsomega.5c00229
ACS Omega 2025, 10, 14229−14240

Limchoowong, N. A Fluorescence Switching Sensor for Sensitive and Selective Detections of Cyanide and Ferricyanide Using Mercuric Cation-Graphene Quantum Dots. *ACS Omega* **2021**, *6* (22), 14379−14393.
(79) Anusuyadevi, K.; Velmathi, S. Design Strategies of Carbon Nanomaterials in Fluorescent Sensing of Biomolecules and Metal Ions -A Review. *Results Chem.* **2023**, *5*, No. 100918.

https://doi.org/10.1021/acsomega.5c00229
ACS Omega 2025, 10, 14229−14240